Tunnel Nitride Passivated Contacts for Silicon Solar Cells Formed by Cat-CVD

Yuli Wen*, Huynh Thi Cam Tu, and Keisuke Ohdaira

Japan Advanced Institute of Science and Technology, Nomi, Ishikawa 923-1292, Japan

E-mail: s2020040@jaist.ac.jp, ohdaira@jaist.ac.jp

An ultra-thin silicon nitride (SiN_x) layer formed by catalytic chemical vapor deposition (Cat-CVD) is used to replace the Si dioxide (SiO_2) layer of a tunnel oxide passivated contact (TOPCon) solar cell. The passivation quality of crystalline Si (c-Si) with a stack of the ultra-thin SiN_x and n-type hydrogenated amorphous Si (a-Si:H) or microcrystalline Si (μc-Si:H), also formed by Cat-CVD, is significantly improved by annealing at 850 °C, probably due to the formation of a back surface field (BSF) layer. Cat-CVD SiN_x with thicknesses of up to 2.5 nm can have sufficient tunneling conduction. The ultra-thin SiN_x having functions of surface passivation and carrier tunneling, and the unification of the formation method for the tunnel SiN_x and conductive layers will lead to the realization of tunnel nitride passivated contact (TNPCon) solar cells.

1. Introduction

Tunnel oxide passivated contact (TOPCon), a kind of passivated contact for crystalline silicon (c-Si) solar cells, is known to have excellent passivation ability despite its simple structure consisting of an ultra-thin tunnel Si oxide (SiO_2) and a P-doped Si layer.[1–4] The ultra-thin tunnel SiO_2 in the TOPCon structure is generally formed by ultraviolet-ozone (UV-O_3) oxidation, thermal oxidation, or wet-chemical oxidation.[5–7] For the tunnel passivated layer, SiO_2 is not the only option, and it has been confirmed that Si nitride (SiN_x) can also work well in passivated contact under appropriate conditions.[8]

There are many methods to form thin tunnel SiN_x films, such as sputtering,[9] jet vapor deposition (JVD),[10,11] atomic layer deposition,[12] plasma-enhanced chemical vapor deposition (PECVD),[13–15] and direct nitridation,[16,17] some of which have been conventionally used in the industry of semiconductor devices.[18,19] Of a variety of methods,

catalytic CVD (Cat-CVD), often also referred to as hot-wire CVD (HWCVD), may be one of the best ways for the formation of thin tunnel SiN_x.[20] Cat-CVD is a method of depositing thin films by decomposing gas molecules on a heated catalyzing wire such as tungsten and tantalum.[21–23] Unlike in the case of PECVD, Cat-CVD can realize plasma-damage-free film deposition, which is suitable for the formation of passivation films on c-Si. We have thus far obtained an outstandingly low surface recombination velocity (SRV) below 5 cm/s when mirror-polished n-type floating-zone (FZ) c-Si wafers are passivated by Cat-CVD SiN_x films with a thickness of ~100 nm.[24] We have also previously demonstrated a good passivation quality of an ultra-thin Cat-CVD SiN_x film covered with a ~8-nm-thick phosphorous (P)-doped Si film, showing an effective minority carrier lifetime (τ_{eff}) of >400 μs.[20]

In this study, we propose a new passivated contact by replacing ultra-thin tunnel SiO_2 in TOPCon with an ultra-thin SiN_x film, named tunnel nitride passivated contact (TNPCon). Although similar structures have been reported,[25] their SiN_x layers do not act as a tunneling passivation film, which is fundamentally different from TNPCon. SiN_x can be formed by one-side deposition by Cat-CVD[26–29], which can be combined with the successive deposition of a P-doped Si layer. As a result, the fabrication process of the cells can be simplified. To investigate the performance of the new passivated contact,[30] the passivation quality of TNPCon was characterized based on minority carrier lifetime. We also evaluated the property of majority carrier transport by resistance measurement. Through these measurements, we demonstrated the feasibility of TNPCon for the passivation contact of c-Si solar cells.

2. Experimental procedures

280 μm-thick, mirror-polished n-type 1–5 Ωcm (100)-oriented FZ Si wafers with a bulk minority carrier lifetime of >10 ms were cleaved into 20×20 mm^2 pieces. All the substrates were cleaned according to the RCA cleaning procedure,[31] then were dipped in 1% hydrofluoric acid (HF) to remove oxide formed during SC-2. After the HF dipping, the substrates were carried into a load lock chamber of a Cat-CVD system immediately. The substrates were then pre-heated up to a target temperature of 200 °C in H_2 atmosphere at 30 Pa for 5 min before the deposition of SiN_x films. The Cat-CVD of SiN_x layers was performed

using a tungsten catalyzer heated at 1800 °C with a length of ~200 cm and a diameter of 0.5 mm placed at a distance of 12 cm from a substrate holder. The samples were set in face-down configuration and four edges of each sample were contacted to the substrate holder. The pressure in the chamber without gas flow was kept in a high vacuum of 10^{-6} Pa. SiN_x layers were deposited symmetrically on both sides of the Si substrates. Except for the investigation on SiN_x thickness dependence, all the SiN_x films were deposited for 10 s, resulting in a SiN_x thickness of ~1.8 nm. Subsequent P-doped microcrystalline Si (μc-Si:H) and amorphous Si (a-Si:H) layers with a thickness of ~20 nm were deposited in another Cat-CVD chamber. μc-Si:H is used mainly in this study, which was formed at a low deposition rate (~4.0 nm/min) under a low SiH_4 flow rate and a high H_2-dilution. a-Si:H films formed at a deposition rate of ~8 nm/min were used for comparison to investigate how the doping concentration of the P-doped Si layer affects the passivation quality of TNPCon. To obtain P-doped μc-Si:H and a-Si:H films with various thicknesses, the deposition duration was systematically varied. The detailed deposition conditions of ultra-thin tunnel SiN_x and P-doped Si layers are summarized in Table I. The thickness of SiN_x and P-doped Si layers were measured on J. A. Woollam HS-190™ spectroscopic ellipsometer. Especially transmission electron microscopy (TEM) images were acquired to confirm the thickness of ultra-thin tunnel SiN_x films more accurately.

The samples with symmetrical TNPCon structures were put into a tube furnace and annealed at 850 °C in N_2 atmosphere for 1 hour. This step is used for the crystallization of precursor μc-Si:H or a-Si:H films and for the diffusion of P in the doped Si layer into a c-Si substrate, to be exact. The crystallization of μc-Si:H and a-Si:H was confirmed by Raman spectroscopy (not shown). In order to investigate the passivation quality of TNPCon on c-Si, the τ_{eff} of the symmetrical samples was measured by microwave photoconductivity decay (μ-PCD) (Kobelco LTA-1510EP) using a laser pulse at a wavelength of 904 nm with a photon density of 5×10^{13} cm^{-2} for the generation of excess carriers.

We prepared two types of structures for the evaluation of the contact resistance of TNPCon structure. Ti/Ag electrodes consisting of ~20 nm-thick Ti and ~1 μm-thick Ag were deposited by vacuum evaporation for both structures. For the structure for the qualitative evaluation of contact resistance, both sides of the 1 cm×1 cm samples were fully covered with the Ti/Ag

electrodes. For the structure for transmission line method (TLM), patterned Ti/Ag electrodes with various intervals were evaporated. Current density–voltage (*J–V*) curves of the samples were measured in a semiconductor analyzer using Kelvin method for these samples to evaluate the tunneling condition of TNPCon structure.

3. Results and discussion

3.1 Thickness dependence of ultra-thin tunnel SiN_x

Figure 1 shows the TEM images of a-Si:H/SiN_x/c-Si structures, in which SiN_x films were deposited for 10 and 30 s, respectively. SiN_x films deposited for 10 and 30 s are 1.7–1.9 nm and 3.1–3.2 nm thick. Hence, the thicknesses of SiN_x films deposited for 20 and 45 s are extrapolated to be ~2.5 and ~4.2 nm, respectively.

Figure 2 shows the *J–V* curves of the samples with various SiN_x thicknesses. In this structure, μc-Si:H formed at a He-diluted PH_3 flow rate of 100 sccm was used as the precursor of P-doped poly-Si. The samples with SiN_x with thicknesses of 1.8 and 2.5 nm show a linear *J–V* curves and have resistances of 0.11 and 0.18 Ωcm^2, respectively. On the other hand, when the thickness of SiN_x increases to 3.2 nm or more, the *J–V* curves lose linearity and resistances increased drastically. This significant change indicates that the tunneling transport of electrons is suppressed as SiN_x thickness increases, and SiN_x with a thickness of up to 2.5 nm has a sufficient carrier tunneling ability. A typical thickness of SiO_2 in TOPCon structure is ~1.5 nm, while the maximum thickness of SiN_x for carrier tunneling was reported to be 2.0 nm.[32] The difference between the maximum thickness for electron tunneling in SiO_2 and SiN_x can be theoretically explained as the result of a lower conduction band offset in SiN_x/c-Si than in SiO_2/c-Si.

Figure 3 shows the τ_{eff} of the samples before and after annealing as a function of SiN_x thickness. The same P-doped layer as the experiment for Fig. 2 was also used in this structure. All the τ_{eff} values increase by annealing, except for the reference sample without a SiN_x layer. This clearly indicates that the ultra-thin SiN_x layer works as a passivation layer. The maximum τ_{eff} of ~0.8 ms was obtained by using an ultra-thin SiN_x with a thickness of 1.8 nm after annealing. On the other hand, as the SiN_x becomes thicker, τ_{eff} after annealing decreases. We also observed a decrease in substrate resistivity (ρ_{sub}), measured on a quasi-

steady-state photoconductance (QSSPC) system, with decreasing SiN_x thickness. During annealing at 850 °C, phosphorus atoms in the doped Si layer are expected to diffuse through the SiN_x layer into c-Si substrate to form a heavily doped n-type Si (n^+-Si) layer, which can explain the decrease of ρ_{sub}. This n^+-Si layer can act as back surface field (BSF), by which its passivation ability is improved. The improvement in τ_{eff} can be explained by the formation of the BSF layer. SiN_x acts as a barrier layer against P-diffusion, and the formation of the BSF layer was suppressed in the samples with thicker SiN_x.

3.2 Doping concentration of P-doped Si

The doping concentration of the P-doped Si on SiN_x can be a crucial factor for the properties of TNPCon since phosphorus in the doped Si layer contributes to the formation of BSF. Here, we compared two types of doped Si precursors: a-Si:H and μc-Si:H. Figure 4 shows the τ_{eff} of the samples with a SiN_x thickness of 1.8 nm as a function of He-diluted PH_3 flow rate. Within a certain range, PH_3 flow rate and phosphorus doping concentration are positively correlated. At the beginning of the increase in doping concentration, both types of Si layers show the same tendency for τ_{eff} improvement, which is consistent with our hypothesis that SiN_x/BSF enhances passivation. TNPCon structures after annealing can realize an excellent passivation ability with a τ_{eff} of ~0.8 ms, independent of the types of P-doped Si precursors. τ_{eff} then turns to decrease with further increase in PH_3 flow rate, the reason for which is unclear at present.

Here we also discuss the τ_{eff} of the samples before high temperature annealing, although this is not the main purpose of this study. In general, an a-Si:H layer shows better passivation ability than μc-Si:H layer, but the difference in τ_{eff} disappears by performing annealing. One plausible explanation is that a-Si:H and μc-Si:H have different passivation mechanisms before annealing, chemical passivation of dangling bonds on c-Si surfaces, while the passivation mechanism is unified into SiN_x/BSF enhanced passivation by high temperature annealing. Combined with the above phenomenon, it is reasonable to speculate that phosphorus doping concentration is one dominating factor in the passivation quality of TNPCon.

3.3 Carrier transport performance of TNPCon

Not only the high passivation quality but good electron transport performance is necessary for the solar cell application of TNPCon. Figure 5 shows the total resistance of the samples for TLM measurement with a SiN_x thickness of 1.8 nm as a function of electrodes interval. All the data points are on the linear fitting line shown as a red dotted line, and the extrapolated zero-length resistance corresponds to the twice of the contact resistance (R_C). R_C of TNPCon is estimated to be only 0.014 Ωcm^2, which is low enough for the utilization to solar cells.

The bare c-Si wafer used in this study has a ρ_{sub} of ~3.5 Ωcm, measured on a QSSPC system. We can also evaluate ρ_{sub} from the slope of the linear fitting line. In Figure 6, ρ_{sub} is estimated to be 1.03 Ωcm, much lower than bare c-Si wafer. In the TLM test, current flows laterally parallel to the plane of the substrate. This indicates that the BSF layer, formed during high temperature annealing by the diffusion of phosphorus atoms from the Si layer, works as a lateral carrier conduction path to reduce a resistance. The lower ρ_{sub} of the sample than that of the Si wafer is a clear experimental evidence for the formation of the BSF layer. Note that lateral carrier flow in poly-Si may be negligible due to air exposure of poly-Si surfaces and resulting carrier depletion by Fermi-level pinning[33].

We also investigated the impact of the thickness of phosphorus-doped Si layer on τ_{eff}. Figure 6 shows the τ_{eff} as a function of the thickness of P-doped Si layer. The P-doped layer here before annealing was ~25-nm-thick μc-Si:H deposited at a PH_3 flow rate of 100 sccm. When the thickness of a P-doped Si layer is >10 nm, τ_{eff} is almost independent of the thickness of the P-doped Si layer. On the other hand, increasing the thickness of P-doped Si layer does not influence the total resistance due to its low resistivity (~10^{-2} Ωcm). We can thus conclude that an extremely thick P-doped Si layer is not necessary for the improvement of the passivation quality of TNPCon.

4. Conclusions

We realized a new type of passivated contact called TNPCon by Cat-CVD with functions of high surface passivation ability and sufficient carrier transport performance. The maximum thickness of Cat-CVD SiN_x for efficient tunneling transport is found to be as thick

as ~2.5 nm. TNPCon shows high passivation ability with a τ_{eff} of ~0.8 ms after high temperature annealing, owing to the formation of a BSF layer as well as the passivation by the ultra-thin SiN_x. Contact resistance of TNPCon is estimated to be 0.014 Ωcm^2, which is low enough to be used for c-Si solar cells. TNPCon is therefore considered as a credible alternative to conventional TOPCon structures.

References

1) F. Feldmann, M. Bivour, C. Reichel, M. Hermle, and S. W. Glunz, Sol. Energy Mater. Sol. Cells **120**, 270 (2014).
2) F. Feldmann, M. Simon, M. Bivour, C. Reichel, M. Hermle, and S. W. Glunz, Appl. Phys. Lett. **104**, 181105 (2014).
3) F. Feldmann, M. Simon, M. Bivour, C. Reichel, M. Hermle, and S. W. Glunz, Sol. Energy Mater. Sol. Cells **131**, 100 (2014).
4) F. Feldmann, M. Bivour, C. Reichel, H. Steinkemper, M. Hermle, and S. W. Glunz, Sol. Energy Mater. Sol. Cells **131**, 46 (2014).
5) A. Moldovan, F. Feldmann, G. Krugel, M. Zimmer, J. Rentsch, M. Hermle, A. R. Folsch, K. Kaufmann, and C. Hagendorf, Energy Procedia **55**, 834 (2014).
6) D. Chen, Y. Chen, Z. Wang, J. Gong, C. Liu, Y. Zou, Y. He, Y. Wang, L. Yuan, W. Lin, R. Yin, L. Yin, X. Zhang, G. Xu, Y. Yang, H. Shen, Z. Feng, and P. P. Altermatt, Sol. Energy Mater. Sol. Cells **206**, 110258 (2020).
7) A. Moldovan, F. Feldmann, M. Zimmer, J. Rentsch, J. Benick, and M. Hermle, Sol. Energy Mater. Sol. Cells **142**, 123 (2015).
8) S. Mitra, H. Ghosh, H. Saha, and K. Ghosh, IEEE Trans. Electron Devices **66**, 1368 (2019).
9) V. Bhatt and S. Chandra, J. Electron. Mater. **38**, 9 (2009).
10) T. P. Ma, IEEE Trans. Electron Devices **45**, 680 (1998).
11) J. P. Han and T. P. Ma, Appl. Phys. Lett. **72**, 1185 (1998).
12) S. Weeks, G. Nowling, N. Fuchigami, M. Bowes, and K. Littau, J. Vac. Sci. Technol, A **34** 01A140 (2016).
13) C. C. Johnson, T. Wydeven, and K. Donohoe, Sol. Energy **31**, 355 (1983).
14) A. G. Prasad, S. M. Dasari, P. Suratkar, and S. Saravanan, Int. J. Electron. Lett. **3**, 87 (2015).
15) T. Lauinger, J. Schmidt, A. G. Aberle, and R. Hezel, Appl. Phys. Lett. **68**, 1232 (1996).
16) A. Izumi, Thin Solid Films **501**, 157 (2006).
17) D. K. Rai, C. S. Solanki, and B. R. Kavaipatti, Mater. Sci. Semicond. Process. **67**, 46 (2017).

18) S. B. Patil, A. Kumbhar, P. Waghmare, V. R. Rao, and R.O. Dusane, Thin Solid Films **395**, 270 (2001).
19) T. Ito, T. Nozaki, H. Arakawa, and M. Shinoda, Appl. Phys. Lett. **32**, 330 (1978).
20) H. Song and K. Ohdaira, Jpn. J. Appl. Phys. **57**, 08RB03 (2018).
21) H. Matsumura and H. Tachibana, Appl. Phys. Lett. **47**, 833 (1985).
22) H. Matsumura, Jpn. J. Appl. Phys. **30**, 1522 (1991).
23) H. Matsumura, Jpn. J. Appl. Phys. **37**, 3175 (1998).
24) T. T. Cham, K. Koyama, K. Ohdaira, and H. Matsumura, Jpn. J. Appl. Phys. **53**, 022301 (2014).
25) D. Yan, A. Cuevas, Y. Wan, and J. Bullock, Phys. Status Solidi RRL **9**, 617 (2015).
26) R. Morimoto, A. Izumi, A. Masuda, and H. Matsumura, Jpn. J. Appl. Phys. **41**, 501 (2002).
27) C. Voz, I. Martin, A. Orpella, J. Puigdollers, M. Vetter, R. Alcubilla, D. Soler, M. Fonrodona, J. Bertomeu, and J. Andreu, Thin Solid Films **430**, 270 (2003).
28) F. Liu, M. Zhu, Y. Feng, Y. Han, and J. Liu, Thin Solid Films **395**, 97 (2001).
29) Y. Matsumoto, S. Godavarthi, M. Ortega, V. Sanchez, S. Velumani, and P.S. Mallick, Thin Solid Films **519**, 4498 (2011).
30) Y. Wen, H. T. C. Tu, and K. Ohdaira, Ext. Abst. 2020 Int. Conf. Solid State Devices and Materials (SSDM2020), 2020, p.401.
31) W. Kern, J. Electrochem. Soc. **137**, 1887 (1990).
32) J. Shewchun, R. Singh, and M. A. Green, J. Appl. Phys. **48**, 765 (1977).
33) M. H. Brodsky, F. Evangelisti, R. Fischer, R. W. Johnson, W. Reuter, and I. Solomon, Solar Cells, **2**, 401 (1980).

Figure Captions

Fig. 1 TEM images of a-Si:H/SiN_x/c-Si structures with SiN_x deposited for 10 and 30 s, respectively.

Fig. 2 *J–V* curves of TNPCon/c-Si/TNPCon structures as a function of SiN_x thickness. Cross-sectional schematic of the TNPCon/c-Si/TNPCon structure for *J–V* measurement is also shown in the inset.

Fig. 3 τ_{eff} of poly-Si/SiN_x/c-Si/SiN_x/poly-Si structures as a function of SiN_x thickness before and after annealing. Cross-sectional schematic of the sample for τ_{eff} measurement is also shown in the inset.

Fig. 4 τ_{eff} of poly-Si/SiN_x/c-Si/SiN_x/poly-Si structures as a function of He-diluted PH_3 flow rate. Two kinds of poly-Si films crystallized from μc-Si:H and a-Si:H are compared. Cross-sectional schematic of the sample for τ_{eff} measurement is also shown in the inset.

Fig. 5 Measured resistance as a function of electrode interval. The dashed line indicates the result of linear fitting. Cross-sectional schematic of sample for TLM measurement is also shown in the inset.

Fig. 6 τ_{eff} as a function of poly-Si thickness. Cross-sectional schematic of the sample for τ_{eff} measurement is also shown in the inset.

Table I. Deposition conditions of ultra-thin tunnel SiN_x and P-doped Si layers (PH_3 is diluted by helium to 2.25%).

	SiN_x	μc-Si:H	a-Si:H
Gas flow rate	SiH_4 3 sccm NH_3 50 sccm H_2 40 sccm	SiH_4 10 sccm H_2 10 sccm PH_3 10–200 sccm	SiH_4 20 sccm PH_3 10–300 sccm
Substrate temperature	200 °C	250 °C	250 °C
Pressure	1.0 Pa	1.0 Pa	1.0 Pa
Catalyzer temperature	1800 °C	1800 °C	1800 °C
Duration	10–45 s	180–600 s	200–240 s

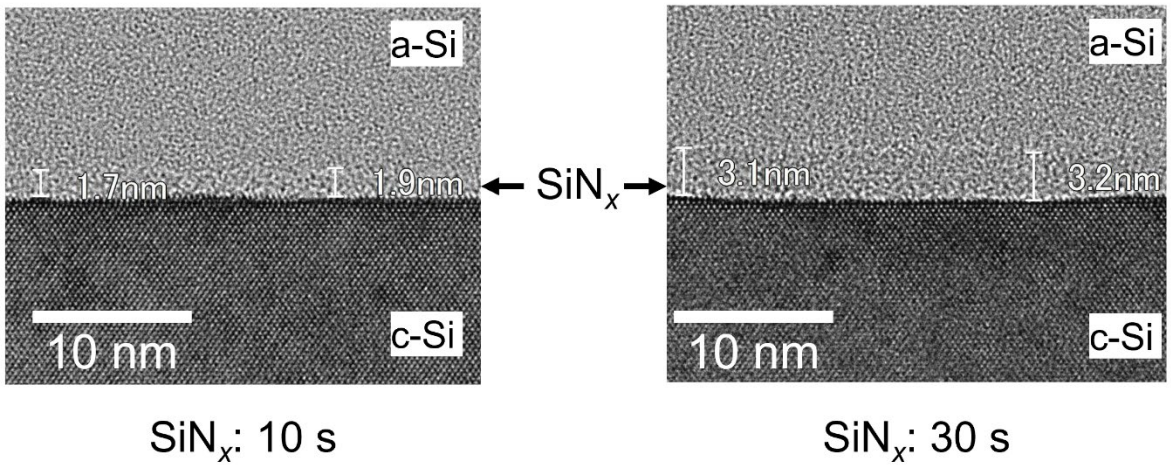

Fig. 1. Y. Wen et al.,

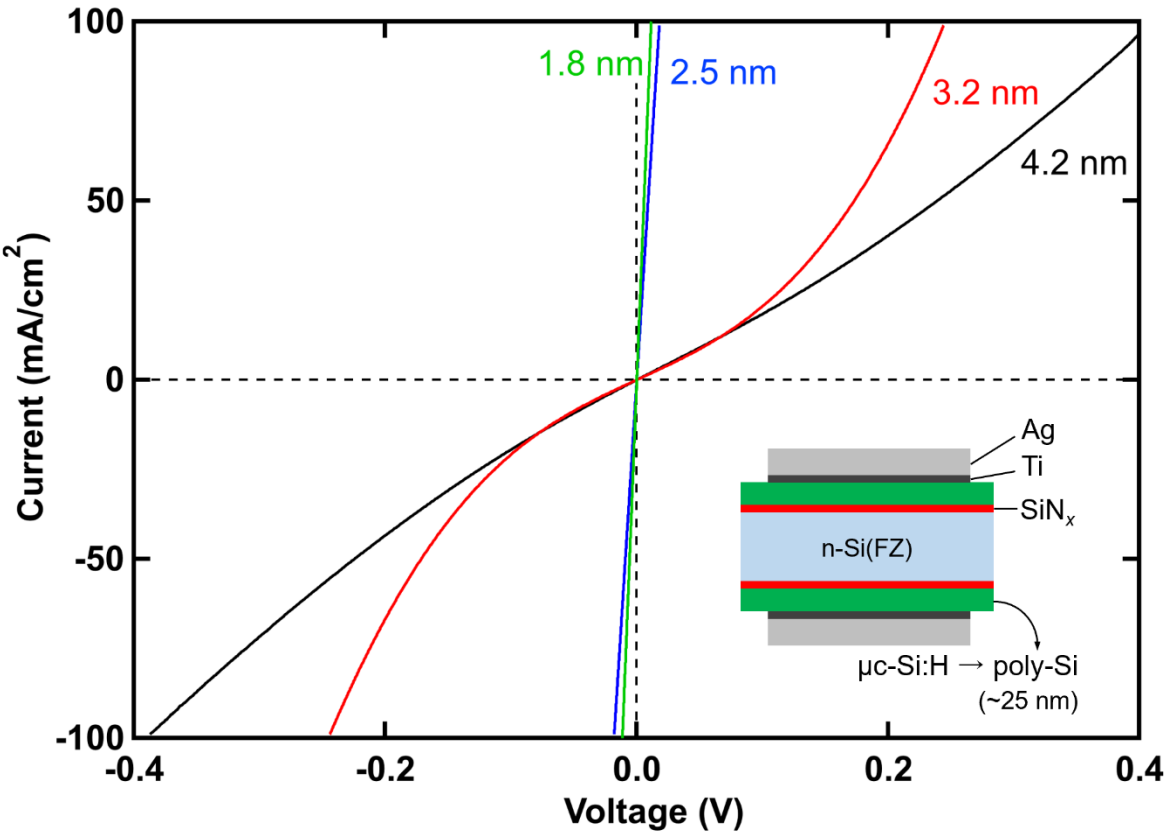

Fig. 2. Y. Wen et al.,

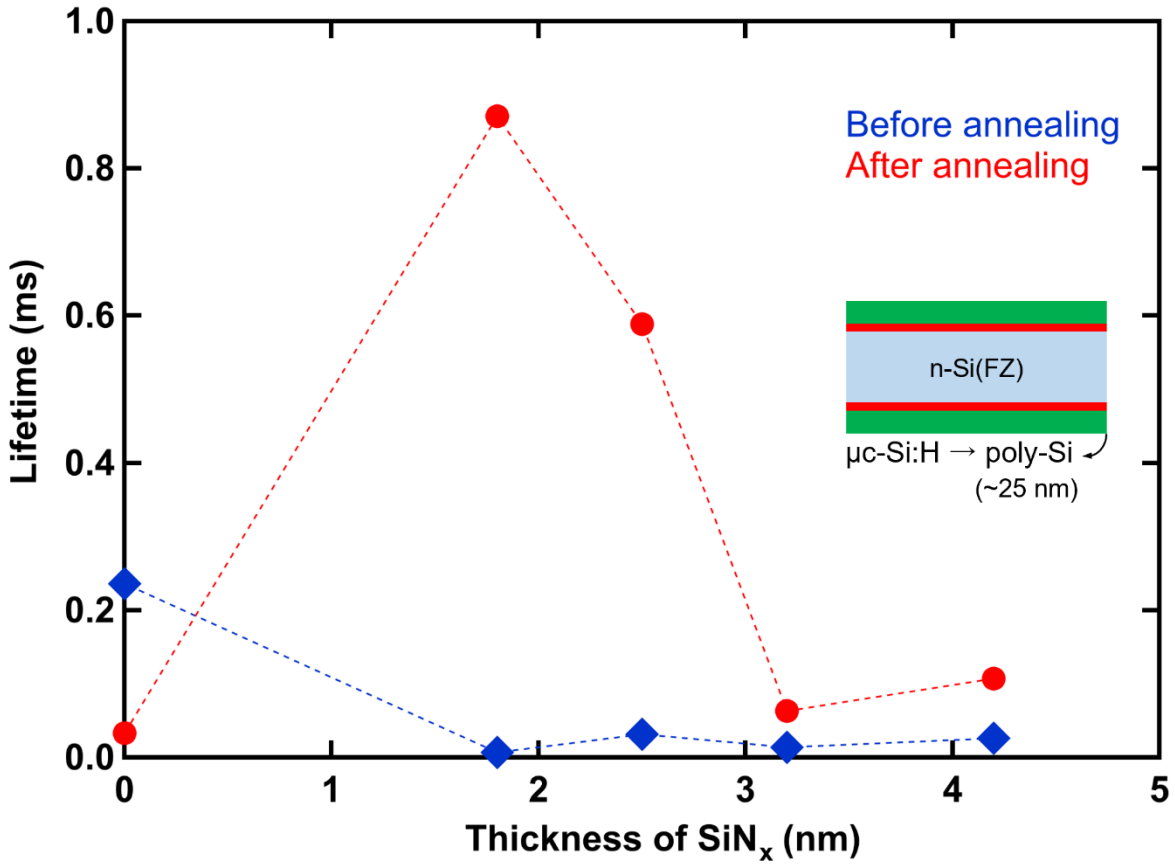

Fig. 3. Y. Wen et al.,

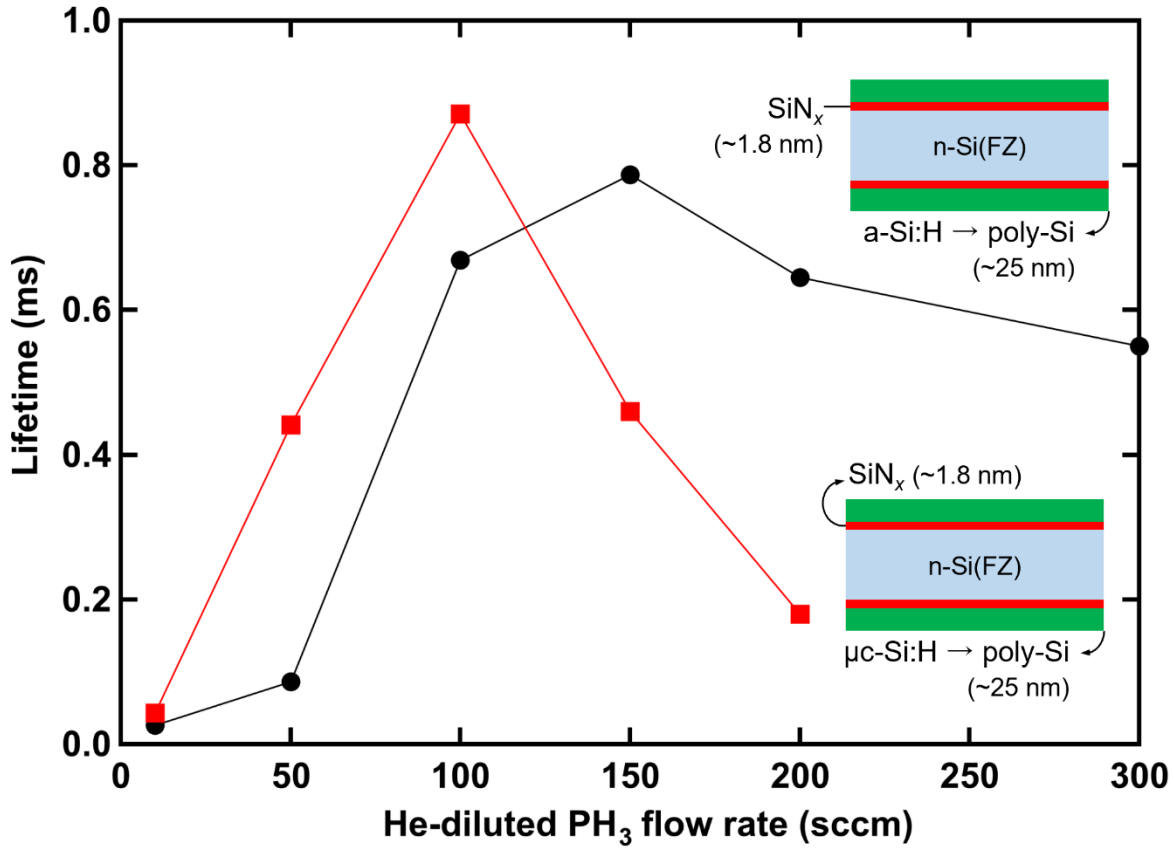

Fig. 4. Y. Wen et al.,

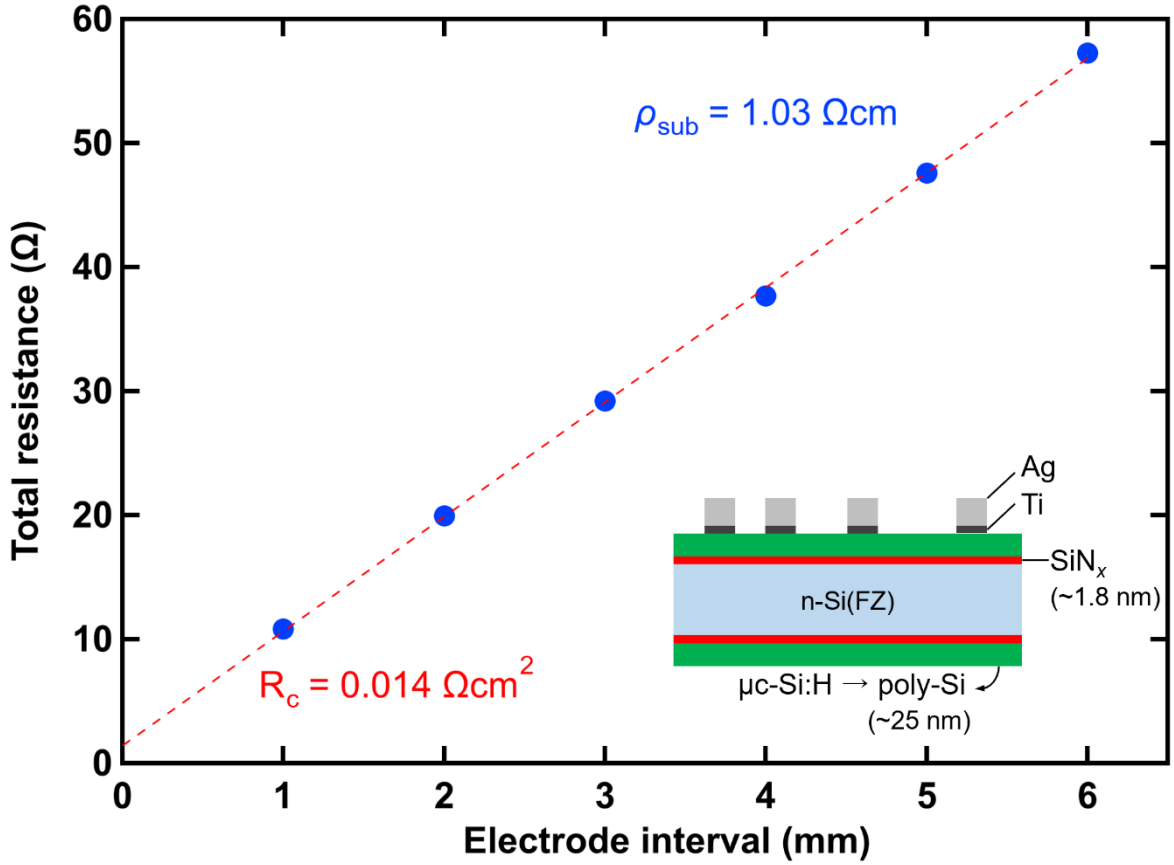

Fig. 5. Y. Wen et al.,

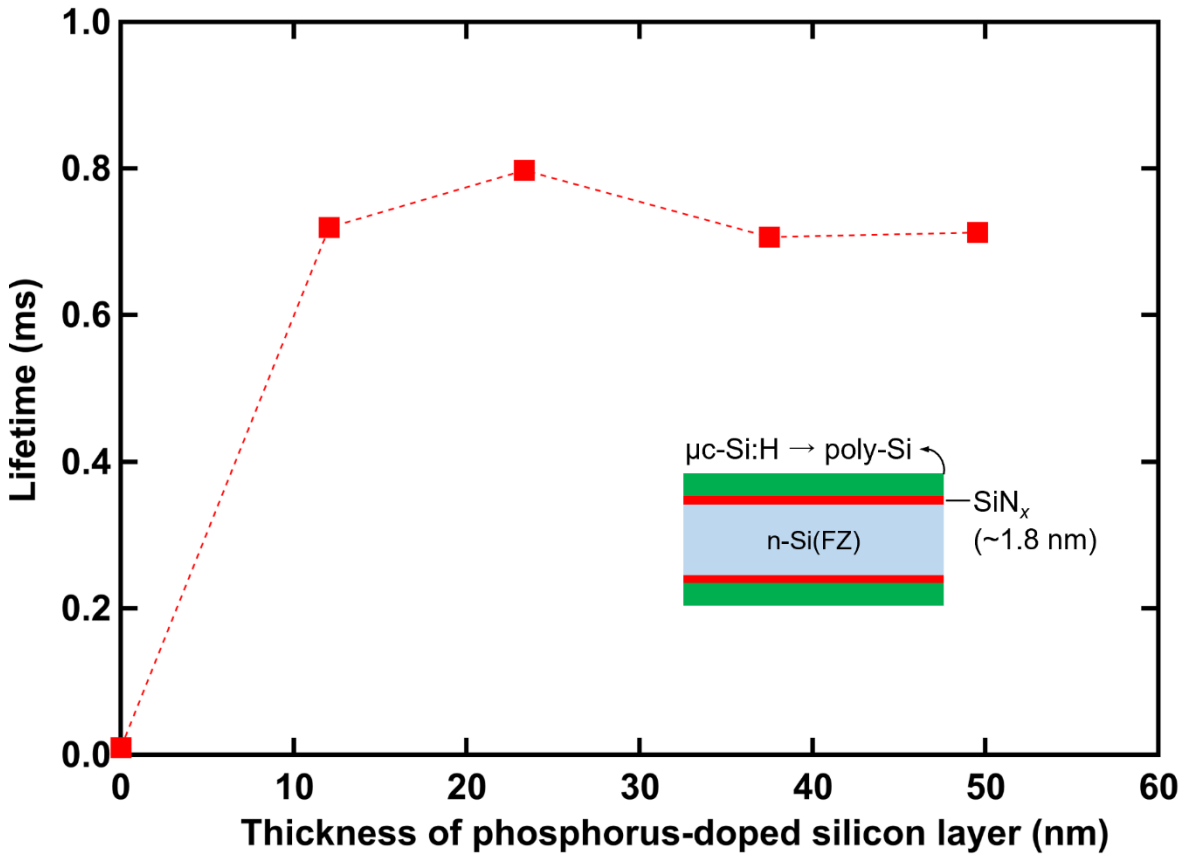

1

2

3 Fig. 6. Y. Wen et al.,